Chapter 2- Literature review

2.1 Photocatalytic degradation of water pollutants: Fundamentals

In photocatalytic process, chemical reaction take place due to interaction between light and photocatalyst. From a microscopic point of view, a photocatalytic degradation process can be divided into four steps: (i) light absorption, (ii) energy conversion (from light energy to electrochemical energy), (iii) recombination, and (iv) oxidation/reduction process [57]. Yet, it is more often indicated from the microscopic perspectives, as shown in Fig. 2.1.

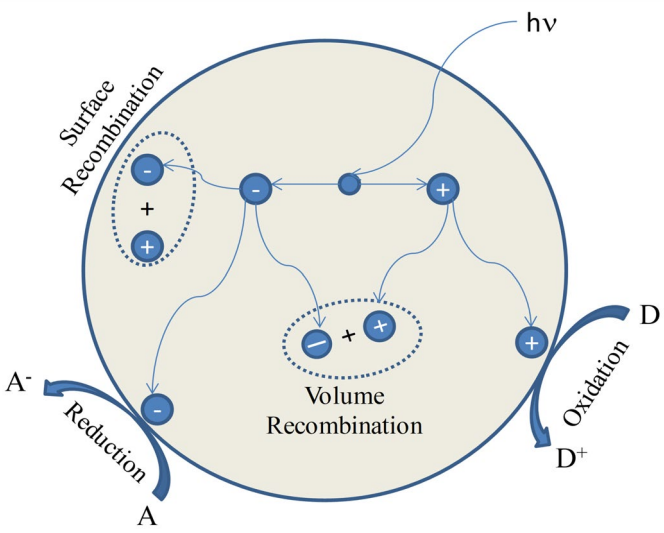

Fig. 2.1 Microscopic phenomena of photocatalytic process [41].

When a semiconductor absorbs light with the energy greater than or equal to its bandgap energy (Eg), a valence electron would be triggered to migrate from valence band to the conduction band, leaving behind a hole on the valence band where the electron used to be (step 1). Electrons and holes generated in this way are powerful reductants and oxidants, respectively, and are almost non-selective to organic, inorganic, and micro-contaminants. The produced electron/hole pairs must separate in order to reach the semiconductor surface and take part in the subsequent reactions (step 2). On the other hand, recombination (step 3), as a rival of separation, is a spontaneous and thermodynamically inevitable process due to the coulomb force between electrons and holes, prohibiting them from reacting with other species in the system. Electrons and

holes that reached the semiconductor surface may oxidize the substrates directly (step 4) or indirectly by producing reactive species such as superoxide radicals and hydroxyl radicals. After multiple steps, the original substrates will be decomposed and mineralized into H_2O, CO_2, and other simple inorganic ions eventually [44].

Photocatalysis for water treatment is usually the oxidative degradation of the substrate pollutants. The mechanism can be classified into two groups according to the functioning reactive species: the direct mechanism is triggered by hole (h^+), while the indirect mechanism is induced by oxidative radicals generated from the interaction between electron (e^-) or hole (h^+) and other dissolved species in the system [58]. The direct oxidation mechanism is also called the hole oxidation mechanism, meaning the organic substrates are oxidized and degraded by photoinduced holes directly. This usually happens when the oxidizing potential of the semiconductor VB is lower than that of the $OH^-/OH^\bullet$ redox pairs and stronger than that of the substrates [59]. The indirect oxidation mechanism is also called the free radical oxidation mechanism, meaning that the organic compounds are oxidized by oxidative radicals, which are normally but not limited to $OH^\bullet$ and $O_2^{-\bullet}$ [60].

The typical participation of holes is indicated by Eq. (2.1-2.9), based on the oxidation potentials of the semiconductor VB and the redox pairs [61].

$$h^+ + H_2O \rightarrow OH^\bullet + H^+ \quad (2.1)$$

$$h^+ + OH^- \rightarrow OH^\bullet \quad (2.2)$$

For photogenerated electrons, it may produce $O_2^{-\bullet}$ via Eq.11 or $OH^\bullet$ going through more complicated processed as revealed by Eq.12 or 13 in an acidic and basic environment, respectively [62, 63].

$$e^- + O_2 \rightarrow O_2^{-\bullet} \quad (2.3)$$

$$O_2^{-\bullet} + e^- + 2H^+ \rightarrow H_2O_2 \quad (2.4)$$

$$H_2O_2 \rightarrow 2OH^{\bullet} \quad (2.5)$$

$$O_2^{-\bullet} + H_2O \rightarrow OH^- + OOH^{\bullet} \quad (2.6)$$

$$OOH^{\bullet} + H^+ \rightarrow OH^{\bullet} + OH^- \quad (2.8)$$

$$OH^- + h^+ \rightarrow OH^{\bullet} \quad (2.9)$$

To further study the mechanism of photocatalytic systems, the active reactive particles must be determined. By comparing the redox potential of band edges and reactive radicals, primary reactive radicals can be predicted theoretically. For example, during the decomposition of benzylic alcohols photocatalysed by Bi_2MoO_6, since the reduction potential of CB (-0.33 eV) was more negative than that of $O_2/O_2^{-\bullet}$ (-0.28 eV), $O_2^{\bullet}$ could be produced by reducing adsorbed O_2 with photo-generated electrons and further decompose the substrates afterward. Due to the more positive oxidation potential of Bi_2MoO_6 VB compared to benzyl alcohol, holes were able to oxidize benzyl alcohol directly. Therefore, the degradation of benzylic alcohols was mainly carried out by $O_2^{-\bullet}$ and h^+ [64].

A more perspicuous way is to apply the quenching experiment. Scavengers with respective to different reactive species are applied separately. The stronger the blocking effect towards photocatalysis, the more important role the corresponding reactive species plays. Reactive species viz., h^+, $O_2^{-\bullet}$ and $OH^{\bullet}$ are generally considered the active free radicals involved in the degradation of organic pollutants [65]. Tian et al. studied degradation of RhB over $SrTiO_3$ modified Bi_2WO_6 composites, it was shown that the photocatalytic activity was significantly inhibited by the addition of EDTA and IPA, indicating the main effects of h^+ and $OH^{\bullet}$, respectively. Therefore, it was concluded that some of the holes generated on Bi_2WO_6 VB flowed to $SrTiO_3$ and directly oxidize RhB, while the rest at the Bi_2WO_6 VB, produced $OH^{\bullet}$ active particles for RhB degradation by OH^- ions oxidation [66].

The kinetics of photocatalytic degradation of aqueous pollutants is still a subject of debate [67]. Most studies argue that the initial rate of reaction is consistent with the pseudo first-order kinetics, which is explained in terms of the modified Langmuir-Hinshelwood model to account for the reactions occurring at the interface of solid/liquid. The effect of the initial substrate concentration on the rate of degradation can be expressed using the following equation:

$$r = -\frac{dC}{dt} = k_r\theta_r = \frac{K_r KC}{1 + KC} \tag{2.10}$$

Where, C is the substrate concentration at an arbitrary time, t is the reaction time, k_r is the reaction rate constant, θ_r is the fraction of catalyst surface area covered by the substrate, and K is the reactant adsorption equilibrium constant. The values of the C and K are typically in the level ppm (mg/L), which makes KC much lower than 1. Therefore, the above equation can be simplified as:

$$-\frac{dC}{dt} = k_r KC = K_{app}C \tag{2.11}$$

Where K_{app} is the apparent reaction rate constant. The term "reaction rate constant" will refer to apparent reaction rate constant of pseudo-first order reaction unless specifically stated. Integrating with the limits of C=C_0 when t=0 and C=C when t=t, where C represents the concentration at any time, Equation (2.11) gives,

$$ln\frac{C_0}{C} = K_{app}t \tag{2.12}$$

Because of the intermediates produced during the reaction, evaluation of photocatalytic efficiency through monitoring of the disappearance rate of initial substrates is not reliable. In this case, the reaction kinetics may be different. Therefore, total organic carbon (TOC) is used as a more convincing parameter to replace the substrate concentration.

Considering that most studies focusing on the organic pollutant degradation upon semiconductor surface follow the pseudo-first-order mechanism, the reaction rate constants involved in this review are apparent reaction rate constants unless stated otherwise.

2.1.1 Key parameters that affect dye degradation

The photocatalytic degradation efficiency of a dye depends on several parameters such as pH, intensity of light, catalyst loading, concentration of dye, and the presence of interfering compounds [90]. The influence of these factors on the degradation properties of the dye is discussed in the following subsections.

2.1.1.1 Effect of catalyst concentration

Catalyst concentration is one of the important parameters in photocatalytic degradation process, and it also accounts for total cost optimization. On increasing catalyst concentration, photocatalytic degradation of water pollutants increases due to increasing electron-hole pair generation. However, on further increasing catalyst concentration degradation efficiency decrease because of increasing turbidity in the solution leading to increasing light scattering and reducing light penetration efficiency [68, 69]. Recently, Anwer et al. [70] examined the catalyst concentration effect on para-nitrophenol (PNP) degradation process and it was found that 250 $mg.L^{-1}$ catalyst concentration showed highest degradation efficiency. The degradation efficiency decreases on increasing catalyst concentration beyond 250 $mg.L^{-1}$.

2.1.1.2 Effect of concentration of water pollutants

Investigation of the effect of initial water pollutants concentration is required to analyse photocatalytic degradation process. However, optimum pollutant concentration greatly dependent on type of pollutant. Generally, on increasing initial pollutant concentration, degradation efficiency increases but on further increasing initial concentration,

degradation efficiency decreases due to limited active site on catalyst surface. Additionally, Some pollutants (especially dyes) absorb more light than a photocatalyst because of that photocatalytic degradation efficiency dropped-off [71]. Li et al. [72] also reported at high initial methyl orange concentration, and degradation efficiency decreases due to reduction of light absorption on catalyst surface. Apart from the factor discussed above, the presence of charges and inorganic metal ions can also affect the photocatalytic degradation efficiency [73].

2.1.1.3 Adsorption of pollutants on the surface of photocatalyst

The pollutants/photocatalyst adsorption is highly dependent on the interaction due to electrostatic force, and binding affinity between pollutants/photocatalyst interface [74]. Sufficient pollutants adsorption on photocatalyst surface and photocatalysis exhibit synergistic effects on degradation efficiency. Generally, composites with good adsorption capacity can utilize simultaneous adsorption and pollutants degradation due to the synergist effect of adsorption and photocatalysis. Anwer et al. [70] has been reported a mechanism for methylene blue degradation and discussed the synergistic effect of adsorption and photocatalytic process. This study reported that after support incorporation, degradation efficiency increases around two-fold relative to photocatalyst alone. However, the adsorption of pollutants is an important parameter but beyond a specific limit can be disadvantageous.

2.1.1.4 Dissolve oxygen

The influence of dissolved oxygen (DO) also affects the photocatalytic degradation process. DO can promote or suppress the efficiency of photocatalytic degradation process depending on reaction mechanism, but it does not affect pollutants adsorption of photocatalyst surface [75]. Shirayama et al. performed photocatalytic degradation experiments in the presence and absence of DO in water and concluded that DO could

act as a scavenger leading to decrease light intensity [76]. Photocatalytic degradation of 2-chlorobiphenyl at various oxygen partial pressure has been studied by Wang and Hong. This study suggested that DO is one of the important reactants in the degradation process [77].

2.1.1.5 Light intensity

Photocatalytic process highly depends on intensity of light and the effect of light on mineralization of water pollutants has been extensively studied [78, 79]. Muruganandham and Swaminathan [80]. studied the light intensity effect on photocatalytic degradation of yellow azo dye, and observed on increasing irradiation intensity from 16 to 62 W, degradation efficiency increases by 33%. An increase in light intensity improves light penetration leading to increased water pollutants degradation efficiency. Although photocatalytic degradation efficiency depends on intensity of light up to a certain limit and beyond this limit, it becomes independent [80-82]. Elaziouti et al. [83] studied the light intensity effect on congo red dye by varying light intensity from 50 to 90 $J.cm^{-2}$ and observed that degradation rate increases up to light intensity 80 $J.cm^{-2}$. Light intensity from 80 to 90 $J.cm^{-2}$ degradation efficiency nearly same and beyond 90 $J.cm^{-2}$ degradation rate start decreases may be due to thermal effects associated with a temperature rise of the solution.

2.1.1.6 Effect of pH

In photocatalytic degradation of water pollutants, pH plays an important role to the photocatalyst surface charge, aggregation of catalyst, and pollutant/catalyst surface interactions [69, 84]. Guettaï et al. [85] studied the effect of pH on photocatalytic degradation of water pollutants and found that degradation rate was highest in acidic medium at pH ~2. Soltani et al. [86] reported that highest degradation efficiency was obtained at pH =2.5. In this study Rhodamine B (RhB) was used as a water pollutant. At

higher pH value, degradation efficiency decreases drastically due to OH^- competition with OOH^- in binding with N^+ of RhB.

2.2 Semiconductor properties for photocatalysis

The energy structure of a given material consists of two energy bands: one is the valence band (VB) filled with valence electrons, and the other is the empty conduction band (CB). For semiconductors, there is an energy gap between the two bands, called the bandgap,

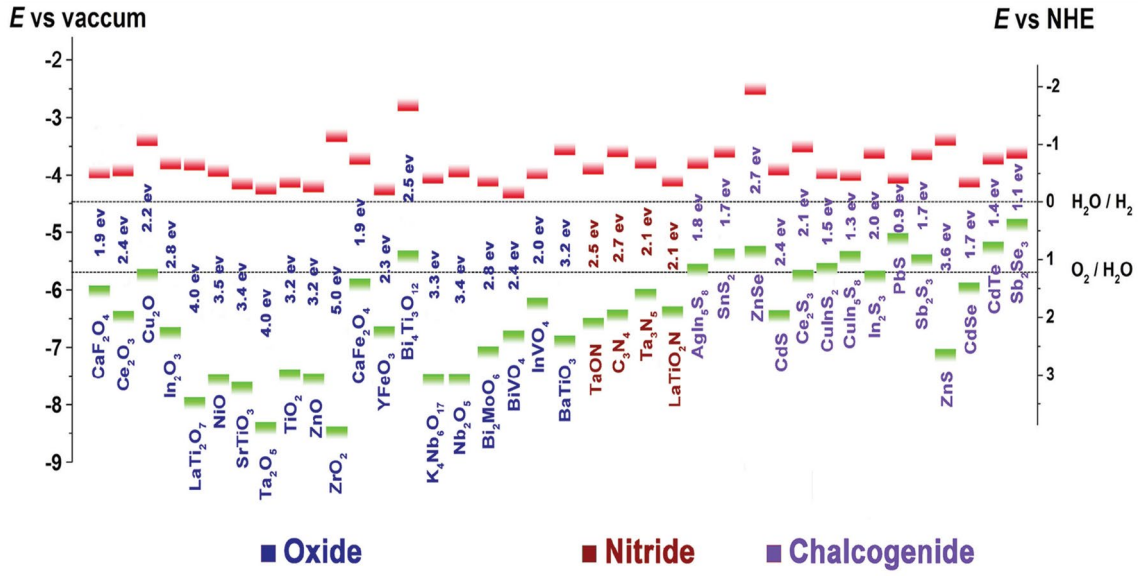

Fig. 3.2 Band edge positions of some semiconductors [115].

in which electrons can transfer from the CB to the VB when triggered by external stimulations such as irradiation in photocatalysis. The CB energy represents the reducing capacity of the semiconductor; the higher (more negative) the CB, the stronger reducing capacity of the semiconductor. Only species (electron acceptors) with lower reduction potential than that of the CB can be reduced. The VB energy, on the other hand, represents the oxidizing capacity; the lower (more positive) the location of the top, the stronger oxidizing capacity of the semiconductor, and only species (electron donors) with an oxidation potential higher than this limitation can be oxidized. In other words, the difference between the energy bands of the semiconductor and the redox potential of the

redox couple determines the possibility for a photocatalytic reaction to happen thermodynamically. Energy band positions and bandgaps of some commonly used semiconductor materials are given in Fig. 2.2.

2.2.1 Energy gap

Energy gap or band gap is an important parameter for a suitable photocatalyst. Electron excited from valance band to conduction band only if absorbed photon energy is greater than bandgap. For a semiconductor, band gap or energy gap can be calculated by the formula proposed by Tauc [87]:

$$\alpha h\nu = A\,(h\nu - E_g)^{n/2} \tag{2.1}$$

where α, h, ν, A, Eg is absorption coefficient, Plank constant, light frequency, a constant, bandgap of the semiconductor respectively, and n is determined by the type of optical transition of a semiconductor (n=1 for direct transition, and for indirect transition n=4). Therefore, the plot of $(\alpha h\nu)^{2/n}$ versus $(h\nu)$ gives bandgap energy of a semiconductor [88]. Although, exact band edge position of the VB and the CB is very difficult, especially in composite materials. Selection of light source highly dependent on band gap energy to avoid wastage of energy and reducing the total cost of wastewater treatment process.

2.2.2 Electron-hole pair recombination

Electron-hole pair recombination in the photocatalyst reduces the degradation efficiency of water pollutants. Photoluminescence is generally used to observe the recombination rate with the assumption that emission light intensity inversely proportional to recombination of electron-hole pair [89]. Photoluminescence emission occurs due to release of electron deexcitation energy from the CB to the VB. If photocatalyst is a composite material, then emission intensity could be misleading because other components (e.g., quantum dots and graphene base material) absorbs or scatters the incident light [90]. Therefore, other methods, viz., circuit potentiometry and radical

scavenging, should be used to analyze recombination of photogenerated electron-hole pairs. However, there is no absolute method present yet for the calculation of electron-hole pair recombination.

2.3 Bismuth ferrite ($BiFeO_3$): A perovskite material

Various materials are used as a photocatalyst but among them, perovskite oxide base materials emerge a promising material for photocatalytic applications. A general formula for ideal perovskite material is ABO_3, and its structure is cubic. The perovskite oxide-based materials have a very large family because most of the metal elements present in periodic table can substitute A site or B site of ABO_3 structure [91]. Substitution of metal induces structural distortion leading to inevitably change in physical, electronic and photocatalytic properties of the base material. Therefore, there are more than two hundred perovskite or perovskite-based materials present. Hence, researchers have shown great interest and devoting more effort to explore ABO_3 type materials by altering the crystal structure and physicochemical properties for photocatalytic applications. ABO_3 type perovskite-based photocatalysts can be classified viz., Titanates (e.g., $CdTiO_3$, $SrTiO_3$, $FeTiO_3$, $BaTiO_3$, $CoTiO_3$, $NiTiO_3$, $CaTiO_3$), Tantalates (e.g., $KTaO_3$, $AgTaO_3$, $NaTaO_3$), Ferrites ($BiFeO_3$, $GdFeO_3$, $LaFeO_3$), and others (e.g., $LaNiO_3$, $LaCaO_3$) [92-104].

Among these materials, $BiFeO_3$ (BFO) is widely used for photocatalytic processes due to several advantages; namely, (i) its band gap suitable for visible spectra, (ii) shows multiferroic behaviour at room temperature leading to efficient electron-hole pair separation, and (iii) highly chemical stable [105-109]. Neel temperature and curie temperature of BFO at room temperature are 370 ^{0}C and 830 ^{0}C, respectively; therefore, it can be easily prepared at room temperature [110, 111]. The BFO shows a distorted rhombohedral structure with R3c space group at room temperature. Its multiferroic behavior introduces many degrees of freedom thus can be used in various fields such as

sensors, volatile memory, piezoelectric devices, and spintronics [112-117]. Additionally, due to its suitable bandgap to harvest solar energy, it is widely used in the field of environmental remediation and water splitting with the help of photocatalytic processes [118, 119].

However, its application is limited in the field of environmental remediation due to the photoinduced electron-hole pairs recombination and lower quantum yield. Several researchers have reported that metal doping, casting nanocomposites, and formation of heterojunctions can improve the photocatalytic activity of BFO.

2.4 Modification of BFO to improve photocatalytic efficiency

The BFO photocatalyst is not commercialized yet for photocatalysis due to mainly its low photocatalytic and quantum efficiency [120]. Various modification methods are used to overcome these issues, viz., doping, surface modification, coupling with carbaneseous material, and heterojunction with other semiconductors.

2.4.1. Rare earth doping

BFO can be modified by introducing other elements in place of A, B, or both sites of the ABO_3 structure leading to alter the multiferroic behavior in order to improve photocatalytic property. To enhance the photocatalytic efficiency of BFO, the choice of the foreign element and its amount is essential. Rare earth metals have some unique properties: electrochemical, luminescent, magnetic, and also ionic radii of most of the rare metals, approximately the same or less than Bi^{+3} ion, which makes it proper choice as a dopant in BFO photocatalyst [120]. Rare-earth metal doping in BFO improves photocatalytic properties of photocatalyst due to mainly structural phase transformation, improving multiferroic behavior, and eliminating secondary phase of BFO [121-123]. Sakar et al. [124] reported visible light active Dy doped BFO nanofibers to degrade methylene blue dye. They observed that Dy mainly altered the bandgap to absorb visible

range light and prevent photo-induced electron-hole pair recombination. Kanwar and Ashish [125] analyze the electromagnetic and phase transformation of BFO on doping Sm in place of Bi^{3+}. They reported that Sm doping eliminates secondary phase of BFO and increases pervoskitic phase. Vanga et al. [126] reported doping of Nd as well as Ni into BFO in place of Bi^{3+} and Fe^{3+} sites, respectively and reported that synergy of co-doping increases photocatalytic efficiency. They concluded that co-dopant decreases electron-hole pairs recombination and increases charge transfer. Various researches on rare earth doped BFO have been carried out, which are reported in Table 2.1.

Table 2. 1 Rare-earth metal doping in BFO for water pollutants.

S.No.	**Rare-earth metal dopant**	**Band gap (e.V)**	**Water pollutant**	**Degradation (%)**	**Ref.**
1	Neodymium	~2.1	RhB	~58% in 180 minutes	[127]
2	Lanthanum	~2.0	Reactive Black-5	~99% in 70 minutes	[128]
3	Ytterbium	~2.1	RhB	~81% in 120 minutes	[129]
4	Dysprosium	~2.3	Methylene Blue	~93% in 240 minutes	[124]
5	Yttrium	~1.6	RhodamineB	~79% in 120 minutes	[130]
6	Gadolinium	~2.3	Methylene Blue	~95% in 240 minutes	[122]

7	Lanthanum & Calcium	~2.1	Methylene blue	~94% in 90 minutes	[131]
8	Neodyium & Nickel	-----	Methylene blue	~94% in 90 minutes	[126]
9	Gadolinium & Tin	~1.4	Congo red	~81% in 120 min	[132]
10	Lanthanum & Selenium	~1.9	Congo red	~81% in 50 min	[120]

2.4.2. Surface modification

Structural change and surface modification in photocatalysts leading effective photocatalytic degradation activity for water pollutants. In order to alter these properties preparation method plays important role [133, 134]. Papdas et al. [135] reported a novel BFO microsphere which is prepared by solvothermal method using chelating agent citric acid. They showed that photocatalyst exhibits highest photocatalytic degradation efficiency may be due to its changed physicochemical behaviour. Huang et al. [134] prepared BFO by microwave-assisted hydrothermal method and varied its morphology by using surfactants like poly vinyl pyrrolidone and ethylenediamine tetraacetic acid. They reported that honeycomb like structure of BFO showed the highest RhB degradation efficiency. The photocatalyst BFO prepared by the electrospinning method improves its paramagnetic behavior leading to improved photocatalytic degradation efficiency [136].

Recently, Liu et al. [137] reported that morphology alteration could enhance production of photoinduced electron-hole pairs and reduce recombination rate leading to improved photocatalytic activity. Wang et al. [138] prepared BFO with tunable morphology by polyvinylpyrrolidone (PVP) assisted hydrothermal method and reported

that PVP control direction of growth in BFO nanostructure. They found that BFO plates with (104) facets exhibit the best photocatalytic activity in methyl orange (MO) degradation process. Moreover, Fei et al. [139] synthesized uniform and pure BFO rods and pill nanoparticles by hydrothermal method. They reported that largely exposed (111) facets show better photocatalytic activity than (111) dominant BFO nanoparticles.

2.4.3. Heterojunction with other materials

Photoinduced charge carrier separation is one of the most important parameters in photocatalytic degradation process. Heterojunction materials exhibit most effective charge carrier separation due to overlapping of two band gaps and also facilitate a passage to transfer the photoinduced charges leading to increased photocatalytic efficiency [140]. Heterojunction forms a Schottky barrier which reduces charge carrier recombination leading to improved photocatalytic activity. Zhang et al. [141] synthesized M@BFO (Ag and Au) composite for RhB degradation process. They reported that noble metals increase near field amplitude of localized surface plasmon leading to efficient charge carrier separation. Niu et al. [142] synthesized Pt co-catlyst modified BFO for water pollutant methyl orange (MO) degradation and they reported that it showed fivefold photocatalytic activity than bare BFO. Heterojunction between Pt and BFO restrain electron-hole pair recombination process leading to better photocatalytic activity.

Luo et al. [143] synthesized $SrTiO_3$ coated BFO and reported that $SrTiO_3$ induces a strong electrostatic field within the material leading to efficient photoinduced charge separation. Therefore, the composite exhibited better photocatalytic activity than the bare BFO. Niu et al. [144] reported $CuO/BiFeO_3$ composite and studied its application on photocatalytic degradation of MO. They reported that p-n type heterostructure was formed, which facilitates efficient electron-hole pair separation leading to better photocatalytic activity. Liu et al. [145] reported a novel $BiFeO_3$–$(Na_{0.5}Bi_{0.5}).TiO_3$ (BFO–

NBT) heterostructure for photocatalytic degradation of RhB. They reported that it shows excellent photocatalytic activity due to well-distributed microstructure and improved multiferroic properties. In summary, heterostructure material significantly improves photocatalytic properties of BFO toward wastewater treatment.

Recently, carbon-based materials have attracted researchers owing to its potential characteristic, viz. thermal stability, high surface area, and high corrosive resistance. Heterojunctions between carbon-based material and the photocatalyst BFO significantly reduce photoinduced electron-hole pair recombination leading to improved photocatalytic activity [146, 147]. Wang et al. [148] reported that graphitic carbon nitride/bismuth ferrite (g-C_3N_4/$BiFeO_3$) composite exhibited high efficiency for MO degradation process. They concluded that formation of heterojunction between g-C_3N_4 and $BiFeO_3$ prevents electron-hole pair recombination and provides a passage to quickly transfer the photogenerated electron leading to better photocatalytic activity. Some of the BFO based heterojunction with other materials (semiconductors and carbonaceous materials) are given in Table 2.2, which are used for the water pollutant degradation process.

Table 2. 2 $BiFeO_3$ based heterojunctions for wastewater treatment.

S.N.	Photocatalyst	Water pollutant	Remarks	Ref.
1.	$BiFeO_3/CuWO_4$	RhB and MO	**Preparation method**: Impregnation **Reaction parameter:** 10 mg catalyst in RhB or MO solution (50 mg. L^{-1}, 50 mL) **Degradation efficiency:** ~87% for MO and ~85% (in 100 min) for RhB	[149]
2.	$Bi_2WO_3/BiFeO_3/g\text{-}C_3N_4$	RhB and TH	**Preperation method**: Sol-gel and hydrothermal **Reaction parameter:** 10 mg catalyst in RhB or TH solution (10 mg. L^{-1}, 100 mL) **Degradation efficiency:** ~84% (in 45 min) for TH and ~99% for (in 30 min) RhB	[150]
3.	$BiFeO_3$@carbon	MO	**Preparation method**: Sol-gel and hydrothermal **Reaction parameter:** 500 mg catalyst in MO solution (20 mg. L^{-1})	[133]

			Degradation efficiency: ~89% for MO (in 180 min)	
4.	M@$BiFeO_3$ (M=Ag, Au)	RhB	**Preparation method**: Sol-gel **Reaction parameter:**500 mg catalyst in RhB solution (10 mg. L^{-1}) **Degradation efficiency:** ~32% for RhB (in 420 min)	[141]
5.	g-C_3N_4/Bi2WO_6	MO	**Preparation method**: Hydrothermal **Reaction parameter:**150 mg catalyst in MO solution (10 mg. L^{-1},50) **Degradation efficiency:** ~100% for MO (in 180 min)	[151]
6.	$BiFeO_3$/TiO_2	RhB	**Preparation method**: Sol-gel and ultrasound immersion **Reaction parameter:** RhB solution (20 mg. L^{-1}) **Degradation efficiency:** ~99% for RhB (in 150 min)	[152]
7.	CuO/$BiFeO_3$	MO and Phenol	**Preparation method**: Hydrothermal and impregnation	[144]

			Reaction parameter: 350 mg catalyst in MO or Phenol solution (5 mg. L^{-1}, 50 mL) **Degradation efficiency:** ~52% for MO and ~50% for Phenol (in 250 min)	
8.	BiFeO3/BiOI	RhB and BPA	**Preparation method**: Hydrothermal and impregnation **Reaction parameter:** 350 mg catalyst in MO or Phenol solution (5 mg. L^{-1}, 50 mL) **Degradation efficiency:** ~52% (in 250 min) for MO and ~50% for Phenol	[153]
9.	$BiFeO_3/ZrO_2$	RhB	**Preparation method**: Sol-gel **Reaction parameter:**100 mg catalyst in RhB solution (20 mg. L^{-1}, 250) **Degradation efficiency:** ~100% for RhB (in 60 min)	[154]
10.	Ag2S/BiFeO3	MO	**Preparation method**: Sol-gel **Reaction parameter:**15 mg catalyst in RhB solution (20 mg. L^{-1})	[155]

			Degradation efficiency: ~100% for RhB (in 240min)	
11.	$BiFeO_3/CuBi_2O_4/BaTiO_3$	NFX	**Preparation method**: Hydrothermal **Reaction parameter:** 20 mg catalyst in NFX solution (10 mg. L^{-1}, 20 mL) **Degradation efficiency:** ~64% for NFX (in 60min)	[156]

2.5 Graphene and its derivatives: A carbon-based material

Graphene is one of the most attractive allotropes for researchers. It is a two-dimensional sheet made of sp2 hybridized carbon in a honeycomb pattern. Geim et al. [157] have reported ground-breaking isolation of graphene from the graphite through scotch tape technique. A number of research papers have been reported on graphene due to its desirable properties, mainly high mechanical strength, high surface area, high electrical conductivity, and high thermal conductivity [158-160].

However, the use of graphene is limited due to several disadvantages like agglomeration in solution, less solubility, and difficult bottom-up synthesis [161, 162]. Therefore, graphene oxide (GO), as an alternative, is used for various applications. It can be synthesized from graphite or other carbon-containing sources, consisting of multiple stacked layers of GO. GO possesses sp^2 hybridized carbon layer stacking and also contains oxygenated functional groups like carboxylic acid, hydroxyl, carbonyl, alkoxy, etc. [163]. Oxygenated functional groups responsible for several advantages, namely surface functionalization possibility and high solubility, open up many opportunities as

compared to graphene. GO can be prepared by oxidizing graphite in presence strong acid (nitric acid and/or sulfuric acid) and very strong oxidizing agent. Among various preparation methods (like Brodie, Staudenmaier, Hoffman method), Hummers-Offeman method is very popular [164].

Oxygenated group present in GO improves properties of graphene mainly in terms of facilitating better aqueous dispersion. However, it decreases delocalization of electrons on sp^2 layered structure due to presence of oxygen, leading to decreased conductivity substantially. Therefore, oxygenated functional groups need to be reduced to enhance the conductivity. After the reduction of the oxygenated group, reduced graphene oxide (rGO) is formed, which has high carbon to oxygen ratio (C/O), leading to high conductivity [165]. Reduced graphene oxide can be produced by treating GO thermally and chemically or by applying both simultaneously. In thermal reduction process, heat is supplied to GO directly or by irradiation (microwave, ultraviolet, infrared) in an inert or reducing environment. A strong reducing agent (viz. sodium borohydride, hydroquinone, hexamethylenetetramine, hydroiodic acid, and Na/K alkaline solutions) is used to produce rGO in chemical reduction method [166].

A promising way of tuning electronic properties of graphene oxide is doping with other elements (nitrogen, phosphorous and sulfur, etc.). Among the dopants, nitrogen doping transfers GO into p- or n-type semiconductor by creating a bandgap, which may act as a co-catalyst for photocatalytic process [167]. Nitrogen doping into graphene results in three nitrogen species as pyrrolic N, pyridinic N, and graphitic N. The pyridinic N is associated with two adjacent C atom of graphene and donate one p-orbital electron into graphene matrix, pyrrolic N donate two p-orbital electrons into graphene system while graphitic N replaces the carbon from the lattices and increases the highest electrical conductivity of graphene. It has a high electron density and high electrical conductivity

[167, 168]. Nitrogen doping into graphene or reduced graphene oxide (rGO) have been done using the following preparation techniques;

I. Chemical Vapor Deposition (CVD)
II. Wet Chemical method
III. Thermal Annealing method
IV. Plasma treatment
V. Arc-discharge method
VI. Solvothermal and hydrothermal method

2.5.1 Graphene-based heterojunctions

Liu et al. prepared rGO wrapped TiO_2 heterojunction by one step photocatalytic reduction technique and reported that rGO capture the photoinduced electron promote photocatalytic performance [169]. Zhang et al. [170] prepared P25/graphene composite for photocatalytic degradation of methylene blue (MB) in water and reported that absorption of MB is increased on catalytic surface than bare P25. Moreover, graphene matrix enhanced photoinduced charge separation and transportation properties leading to increased photocatalytic efficiency.

Li et al. [147] synthesized graphene based BFO nano hybrids as a photocatalyst for congo red (CR) degradation process. They reported that carbon of graphene chemically interacted with BFO providing a passage to transport the electrons, suppress the recombination of electron-hole pair leading to six-fold photocatalytic efficiency than bare BFO. Si et al. [171] also reported BFO/graphene composite for photocatalytic degradation of MB. They concluded that graphene enhances optical properties and prevents photogenerated electron-hole pair recombination. Some of the studies based on graphene-based composite for treatment of water pollutants are given in Table 2.3.

Table 2. 3 Graphene-based composites for degradation of water pollutants.

S.N.	Photocatalyst	Water pollutant	Remarks	Ref.
1.	TiO_2/Graphene	MB	**Preparation method**: Sol-gel **Reaction parameter:** catalyst loading - 100 mg. L^{-1} MB solution ($1x10^{-5}$ M) **Degradation efficiency:** ~75% (in 180 min)	[172]
2.	ZnO@Graphene	RhB	**Preparation method**: Hydrothermal **Reaction parameter:** catalyst loading - 30 mg. L^{-1} RhB solution (10 mg. L^{-1}) **Degradation efficiency:** ~100% (in 600 min)	[173]
3.	Bi_2WO_6/Graphene	RhB	**Preparation method**: In situ-hydrothermal **Reaction parameter:** catalyst loading - 100 mg. L^{-1} RhB solution (100 mL, 10^{-5} M) **Degradation efficiency:** ~100% (in 8 min)	[174]

4.	$ZnFe_2O_4$/Graphene	MB	**Preparation method**: Hydrothermal **Reaction parameter:** catalyst loading - 500 mg. L^{-1} MB solution (100 mL, 20 mg. L^{-1}) **Degradation efficiency:** ~99% (in 90 min)	[175]
5.	Bi_2WO_6/rGO	RhB	**Preparation method**: Hydrothermal **Reaction parameter:** catalyst loading - 500 mg. L^{-1} RhB solution (200 mL, 60 mg. L^{-1}) **Degradation efficiency:** ~100% (in 240 min)	[176]
6.	WO_3/rGO	SMX	**Preparation method**: Hydrothermal **Reaction parameter:** catalyst loading - 400 mg. L^{-1} SMX solution (100 mL, 10 mg. L^{-1}) **Degradation efficiency:** ~98% (in 180 min)	[177]

7.	Bi_2MoO_6/N-rGO	MB	**Preparation method**: Hydrothermal and solgel **Reaction parameter:** catalyst loading - 500 mg. L^{-1} MB solution (100 mL,10 mg. L^{-1}) **Degradation efficiency:** ~98% (in 90 min)	[178]
8.	$BiVO_4$/N-rGO	MB	**Preparation method**: Hydrothermal **Reaction parameter:** catalyst loading - 50 mg. L^{-1} MB solution (100 mL, $3x10^{-5}$ M) **Degradation efficiency:** ~98% (in 240 min)	[179]
9.	ZnO/N-rGO	DCP	**Preparation method**: Solvothermal **Reaction parameter:** catalyst loading - 1200 mg. L^{-1} DCP solution (100 mL, 10 mg. L^{-1}) **Degradation efficiency:** ~60% (in 120 min)	[180]

10	$CdIn_2S_4$/N-rGO	DCP	**Preparation method**: Hydrothermal **Reaction parameter:** catalyst loading - 500 mg. L^{-1} DCP solution (100 mL, 50 mg. L^{-1}) **Degradation efficiency:** ~80% for (in 360 min)	[181]
11.	BiOI/N-rGO	RhB	**Preparation method**: Hydrothermal **Reaction parameter:** catalyst loading - 1000 mg. L^{-1} RhB solution (100 mL, 50 mg. L^{-1}) **Degradation efficiency:** ~82% for (in 90 min)	[182]

2.6 Sonophotocatalytic process: Ultrasound assisted photocatalysis

Photocatalysis and sonolysis both are useful technique in environmental remediation process. However, combining sonolysis with photocatalytic process, which is called sonophotocatalytic process, exhibits synergistic effect in wastewater pollutant degradation process. In sonophotocatalytic process, pollutant degradation rate could be higher than or equal to sum of individual degradation rate [183]. In sonophotocatalytic degradation process, generation of free radicals is more than the individual irradiation (UV and ultrasound) which is main ingredient to break the water pollutants leading to

increasing degradation rate. Ultrasound responsible for cavitation in the solution which not only produce free radical but also promote segregation of catalyst leading to enhanced degradation rate. Sonophotocatalytic efficiency for water pollutant degradation can be ascribed to following: (i) $OH^{\bullet}$ radicals produce by cavitation (ii) regeneration of active sites of catalyst due to cavitation (iii) acoustic cavitation prevent catalyst agglomeration leading to increased surface area for pollutant adsorption and (iv) hydrophobic pollutant can degrade inside cavity [184]. The above effects due to cavitation leading to synergy in order to water pollutant degradation. However, synergy, as well as degradation efficiency highly dependent on acoustic frequency and studied, showed that at low acoustic frequency snophotocatalysis resulted stronger synergistic effect [54]. Ahmad et al. studied sonophotocatalytic degradation of RhB in presence of MWCNTs-ZnO nanocomposite. They reported that the apparent reaction rate constant for sonophotocatalysis is greater than the sum of reaction rate constants of individual processes at low (35 kHz) acoustic frequency. Table 2.4 shows a brief study on sonophtocatalytic degradation processes for water pollutant.

Table 2. 4 Sonophotocatalytic processes for wastewater treatment.

S.N.	Catalyst	Water pollutant	Remarks	Ref.
1.	ZnO/CNTs	RhB	**Catalyst loading:** 30 mg in 30 mL solution **Pollutant concentration:** 20 mg. L^{-1} **Sonophotocatalytic degradation:** ~84% in 60 min	[185]
2.	TiO_2	2-CLP	**Catalyst loading:** 100 mg. L^{-1} **Pollutant concentration:** $5x10^{-4}$ mol. L^{-1} **Sonophotocatalytic degradation:** ~70% in 200 min	[186]
3.	TiO_2	RR	**Catalyst loading:** 300 mg. L^{-1} **Pollutant concentration:** 50 mg. L^{-1} **Sonophotocatalytic degradation:** ~90% in 150 min	[187]
4.	ZnO	Phenol	**Catalyst loading:** 30 mg in 30 mL solution **Pollutant concentration:** 20 mg. L^{-1} **Sonophotocatalytic degradation:** ~84% in 120 min	[188]
5.	WO3/CNT	TTC	**Catalyst loading:** 70 mg. L^{-1} **Pollutant concentration:** 60 mg. L^{-1}	[189]

			Sonophotocatalytic degradation: ~98% in 60 min	
6.	Ag/TiO_2	MO	**Catalyst loading:** 36 mg. L^{-1} **Pollutant concentration:** 32 mg. L^{-1} **Sonophotocatalytic degradation:** ~94% in 120 min	[190]
7.	ZnO	RhB	**Catalyst loading:** 50 mg. L^{-1} **Pollutant concentration:** 10 mg. L^{-1} **Sonophotocatalytic degradation:** ~78% in 120 min	[191]
8.	ZnO/MK_{10}	MB	**Catalyst loading:** 100 mg. L^{-1} **Pollutant concentration:** 20 mg. L^{-1} **Sonophotocatalytic degradation:** ~67% in 120 min	[192]
9	Bi_2WO_6	RhB	**Catalyst loading:** 50 mg. L^{-1} **Pollutant concentration:** 100 mg. L^{-1} **Sonophotocatalytic degradation:** ~99% in 90 min	[193]
10	Tb-CdSe	RB5	**Catalyst loading:** 1000 mg. L^{-1} **Pollutant concentration:** 20 mg. L^{-1}	[194]

			Sonophotocatalytic degradation: ~80% in 60 min	
11.	ZnO/Graphene	4-NP	**Catalyst loading:** 50 mg in 100 mL **Pollutant concentration:** 10 mg. L^{-1} **Sonophotocatalytic degradation:** ~60% in 180 min	[195]
12.	N/Ti codoped TiO_2/Bi_2WO_6	RhB	**Catalyst loading:** 7.5 mg in 15 mL **Pollutant concentration:** 20 mg. L^{-1} **Sonophotocatalytic degradation:** ~97% in 50 min	[196]
13.	rGO/g-C_3N_4	TC	**Catalyst loading:** 10 mg in 40 mL **Pollutant concentration:** 20 mg. L^{-1} **Sonophotocatalytic degradation:** ~90% in 60 min	[197]
14.	$FeVO_4$@BiOCl	4-NP	**Catalyst loading:** 100 mg in 1000 mL **Pollutant concentration:** 20 mg. L^{-1} **Sonophotocatalytic degradation:** ~97% in 40 min	[198]